J|A|C|S
ARTICLES
Published on Web 06/19/2002

Mutual Control of Axial and Equatorial Ligands: Model Studies with [Ni]-Bacteriochlorophyll-*a*

Roie Yerushalmi,[†,‡] Dror Noy,[†,§] Kim K. Baldridge,[||] and Avigdor Scherz*[,‡]

Contribution from the Department of Plant Sciences, The Weizmann Institute of Science, 76100 Rehovot, Israel, and Department of Chemistry, University of California, San Diego, California

Received September 4, 2001

Abstract: Modification of the metal's electronic environment by ligand association and dissociation in metalloenzymes is considered cardinal to their catalytic activity. We have recently presented a novel system that utilizes the bacteriochlorophyll (BChl) macrocycle as a ligand and reporter. This system allows for charge mobilization in the equatorial plane and experimental estimate of changes in the electronic charge density around the metal with no modification of the metal's chemical environment. The unique spectroscopy, electrochemistry and coordination chemistry of [Ni]-bacteriochlorophyll ([Ni]-BChl) enable us to follow directly fine details and steps involved in the function of the metal redox center. This approach is utilized here whereby electro-chemical reduction of [Ni]-BChl to the monoanion [Ni]-BChl$^-$ results in reversible dissociation of biologically relevant axial ligands. Similar ligand dissociation was previously detected upon photoexcitation of [Ni]-BChl (Musewald, C.; Hartwich, G.; Lossau, H.; Gilch, P.; Pollinger-Dammer, F.; Scheer, H.; Michel-Beyerle, M. E. *J. Phys. Chem. B* **1999**, *103*, 7055−7060 and Noy, D.; Yerushalmi, R.; Brumfeld, V.; Ashur, I.; Baldridge, K. K.; Scheer, H.; Scherz, A. *J. Am. Chem. Soc.* **2000**, *122*, 3937−3944). The electrochemical measurements and quantum mechanical (QM) calculations performed here for the neutral, singly reduced, monoligated, and singly reduced, monoligated [Ni]-BChl suggest the following: (a) Electroreduction, although resulting in a π anion [Ni]-BChl$^-$ radical, causes electron density migration to the [Ni]-BChl core. (b) Reduction of nonligated [Ni]-BChl does not change the macrocycle conformation, whereas axial ligation results in a dramatic expansion of the metal core and a flattening of the highly ruffled macrocycle conformation. (c) In both the monoanion and singly excited [Ni]-BChl ([Ni]-BChl*), the frontier singly occupied molecular orbital (SOMO) has a small but nonnegligible metal character. Finally, (d) computationally, we found that a reduction of [Ni]-BChl·imidazole results in a weaker metal−axial ligand bond. Yet, it remains weakly bound in the gas phase. The experimentally observed ligand dissociation is accounted for computationally when solvation is considered. On the basis of the experimental observations and QM calculations, we propose a mechanism whereby alterations in the equatorial π system and modulation of σ bonding between the axial ligands and the metal core are mutually correlated. Such a mechanism highlights the dynamic role of axial ligands in regulating the activity of metal centers such as factor F430 (F430), a nickel-based coenzyme that is essential in methanogenic archea.

Introduction

The catalytic action of biological metal centers frequently involves changing the coordination sphere of the metal, by breaking and forming coordinative bonds with protein residues, substrates, or other small molecules (e.g., CO, O_2, NO, or water). Presumably, the dynamical effect of this process modulates the electronic properties and coordination chemistry of the metal and thereby its activity throughout the catalytic cycle.[3−6] The coordination properties of a particular metal in different electronic states may be utilized for triggering substrate binding and release as well as to mediate protein conformational changes.[6−12]

* To whom correspondence should be addressed. E-mail: avigdor.scherz@weizmann.ac.il.
[†] In partial fulfillment of Ph.D. Thesis.
[‡] Weizmann Institute of Science.
[§] Present address: Biochemistry and Biophysics Dept., University of Pennsylvania.
[||] University of California.

(1) Musewald, C.; Hartwich, G.; Lossau, H.; Gilch, P.; Pollinger-Dammer, F.; Scheer, H.; Michel-Beyerle, M. E. *J. Phys. Chem. B* **1999**, *103*, 7055−7060.
(2) Noy, D.; Yerushalmi, R.; Brumfeld, V.; Ashur, I.; Baldridge, K. K.; Scheer, H.; Scherz, A. *J. Am. Chem. Soc.* **2000**, *122*, 3937−3944.
(3) Hall, J. F.; Kanbi, L. D.; Harvey, I.; Murphy, L. M.; Hasnain, S. S. *Biochemistry* **1998**, *37*, 11451−11458.
(4) Hall, J. F.; Kanbi, L. D.; Strange, R. W.; Hasnain, S. S. *Biochemistry* **1999**, *38*, 12675−12680.
(5) Malmstrom, B. G.; Wittung-Stafshede, P. *Coord. Chem. Rev.* **1999**, *186*, 127−140.
(6) Sharp, R. E.; Chapman, S. K. *Biochim. Biophys. Acta* **1999**, *1432*, 143−158.
(7) Poulos, T. L. *Nat. Struct. Biol.* **1996**, *3*, 401−403.
(8) Williams, P. A.; Fulop, V.; Garman, E. F.; Saunders, N. F. W.; Ferguson, S. J.; Hajdu, J. *Nature* **1997**, *389*, 406−412.
(9) Pascher, T.; Chesick, J. P.; Winkler, J. R.; Gray, H. B. *Science* **1996**, *271*, 1558−1560.
(10) Wittung-Stafshede, P.; Lee, J. C.; Winkler, J. R.; Gray, H. B. *Proc. Natl. Acad. Sci. U.S.A.* **1999**, *96*, 6587−6590.
(11) Wittung, P.; Malmstrom, B. G. *Febs Lett.* **1996**, *388*, 47−49.

10.1021/ja0121078 CCC: $22.00

Scheme 1

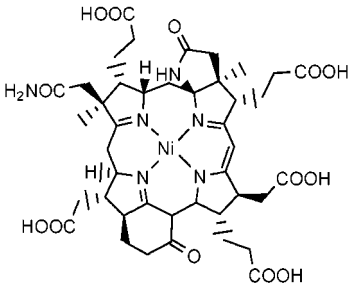

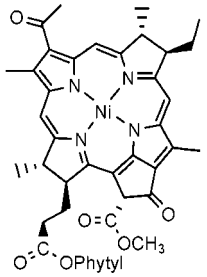

Two types of coordinative bonds to a metal center are usually observed: kinetically stable bonds that are kept fixed, and weaker bonds that allow for easy exchange of ligands (e.g., substrate molecules). Amino acid residues (such as histidine, tyrosine, aspartic and glutamic acids, methionine, and cysteine) most commonly function as ligands of the second type in metalloenzymes. Bonds of the first type are manifested by the tetrapyrrole macrocycles, which make kinetically stable complexes with different metal ions. In this case, the four pyrroles are arranged around the metal in a quasi-planar geometry, leaving two axial positions free for binding protein residues or substrate molecules, or both.

Metallotetrapyrroles such as hemes, chlorophylls, and cobalamins are among the most important and most extensively studied bioinorganic compounds,[13] because of their vital role in different redox reactions. They are also useful for modeling general metal−ligand interactions because: (1) their characteristic $\pi-\pi^*$ absorption spectrum is a useful marker that is sensitive to the redox and coordination state of the central metal; (2) a wealth of data concerning structure and structure−function relationships of metalloporphyrin-containing proteins is currently available; (3) while the chemical environment created by the equatorial tetrapyrrole ligand is kept fixed, both in vivo and in vitro, the axial positions are free for interaction with additional ligands; and (4) chemical methods for preparing a wide variety of complexes with different macrocycles, peripheral substituents, and central metals are well established.[14]

Synthetic nickel porphyrins ([Ni]-porphyrins) have been extensively used for modeling hemes.[15−17] The discovery of nickel-containing porphyrinic biomolecules, such as tunichlorin, a metabolite of marine invertebrates[18,19] and in particular, factor F430 (F430, Scheme 1), scores the significance of [Ni]-porphyrins as realistic models for the activity of nickel in vivo. F430 is a highly saturated [Ni]-porphyrin derivative ([Ni]-dodecahydroporphyrin) that is incorporated into the active site of methyl coenzyme M reductase (MCR), a key enzyme common to all methanogenic archea. The enzyme catalyzes the final step of methane formation from CO_2 in a catalytic cycle that involves the Ni(I) and Ni(II) redox states.[20−22]

A major open question, with respect to the F430 activity, concerns the involvement of axial ligands in the conversion of the inactive MCR_{silent} (a Ni(II) complex) to the "ready" (MCR_{ox1}) and activated (MCR_{red1}) complexes.[21] Specifically, Telser et al. suggest that the transition from MCR_{silent} to MCR_{red1} involves a full or partial dissociation of one of the axial ligands. This point is also related to the role played by the F430 geometry in controlling the catalytic cycle.[21] Although recent computational studies emphasized the contribution of peripheral substituting groups to the macrocycle conformation,[23] experimental data point at a significant interplay of axial ligation association, MCR activation,[20,21,24] and the dynamic coordination sphere during the catalytic cycle. In addition, recent X-ray studies at atomic resolution showed substantial differences in both axial ligation and binding of the porphyrin ligand to the protein when $MCR_{Ox1-silent}$ was compared to $MCR_{Red1-silent}$. Since these two conformations are related to different steps of the catalytic cycle, the observed modifications may provide additional evidence for the role played by the ligand in controlling the activity of the Ni center.

Different aspects of Ni−ligand interactions can be studied using Ni− substituted bacteriochlorophyll ([Ni]-BChl, Scheme 1). Our present study of [Ni]-BChl provides insight to the interplay of charge distribution around the metal, and coordination chemistry. We found interesting similarities in the coordination chemistry of F430 and [Ni]-BChl. These similarities provide a lead to the possible role of ligand in F430 activity.

Initial estimates of metal−ligand charge mobilization, as outlined and applied to [Ni]-BChl in our previous works[2,25,26] led us to expect ligand association/dissociation to depend on the amount of excess charge at the metal core, regardless of specific details of orbital symmetry. More specifically, we expected a unified mechanism to account for ligand dissociation from either the excited or reduced ground states.

Here, we tested this idea by investigating the effect of electroreduction on the coordination properties of [Ni]-BChl with three nitrogenous axial-ligands: 1-methyl-imidazole (1MeIm), *N*,*N*-dimethylaminopyridine (DMAP), and pyridine (Py). Experimentally, we showed that the ligands dissociate upon reduction of neutral [Ni]-BChl to [Ni]-$BChl^-$, the monoanion. Computationally, we provide a detailed description of charge density distribution in the species of [Ni]-BChl discussed here. The combination of experimental and computational approaches allowed us to decipher the solvent role in the observed ligand dissociation. On the basis of these findings we discuss the connection between charge density and ligand coordination

(12) Wittung-Stafshede, P.; Malmstrom, B. G.; Winkler, J. R.; Gray, H. B. *J. Phys. Chem. A* **1998**, *102*, 5599−5601.
(13) Kaim, W.; Schwederski, B. *Bioinorganic Chemistry: Inorganic Elements in the Chemistry of Life*; Wiley: New York, 1994.
(14) Smith, K. M. *Porphyrins and Metalloporphyrins*; Elsevier: Amsterdam, 1975.
(15) Shelnutt, J. A.; Song, X. Z.; Ma, J. G.; Jia, S. L.; Jentzen, W.; Medforth, C. J. *Chem. Soc. Rev.* **1998**, *27*, 31−41.
(16) Shibayama, N.; Yonetani, T.; Regan, R. M.; Gibson, Q. H. *Biochemistry* **1995**, *34*, 14658−14667.
(17) Ma, J. G.; Laberge, M.; Song, X. Z.; Jentzen, W.; Jia, S. L.; Zhang, J.; Vanderkooi, J. M.; Shelnutt, J. A. *Biochemistry* **1998**, *37*, 5118−5128.
(18) Dolphin, D.; Traylor, T. G.; Xie, L. Y. *Acc. Chem. Res.* **1997**, *30*, 251−259.
(19) Sings, H. L.; Bible, K. C.; Rinehart, K. L. *Proc. Natl. Acad. Sci. U.S.A.* **1996**, *93*, 10560−10565.
(20) Telser, J.; Horng, Y. C.; Becker, D. F.; Hoffman, B. M.; Ragsdale, S. W. *J. Am. Chem. Soc.* **2000**, *122*, 182−183.
(21) Telser, J.; Davydov, R.; Horng, Y. C.; Ragsdale, S. W.; Hoffman, B. M. *J. Am. Chem. Soc.* **2001**, *123*, 5853−5860.
(22) A Ni(III) redox state was also proposed as a catalytic transient. However, recent EPR and ENDOR studies contradict this assumption. See: Telser, J.; Horng, Y. C.; Becker, D. F.; Hoffman, B. M.; Ragsdale, S. W. *J. Am. Chem. Soc.* **2000**, *122*, 182−183.
(23) Wondimagegn, T.; Ghosh, A. *J. Am. Chem. Soc.* **2000**, *122*, 6375−6381.
(24) Grabarse, W.; Mahlert, F.; Duin, E. C.; Goubeaud, M.; Shima, S.; Thauer, R. K.; Lamzin, V.; Ermler, U. *J. Mol. Biol.* **2001**, *309*, 315−330.
(25) Noy, D.; Fiedor, L.; Hartwich, G.; Scheer, H.; Scherz, A. *J. Am. Chem. Soc.* **1998**, *120*, 3684−3693.
(26) Noy, D. *An Electrochemical and Spectroscopic Investigation of Metal Substituted Chlorophylls and Bacteriochlorophylls*; Weizmann Institute of Science, Israel, 1995.

around the metal center in [Ni]-BChl. The derived principles are proposed to apply for catalytic metal centers in general and the F430 center in particular.

Materials and Methods

Materials. [Ni]-BChl was prepared according to Hartwich et al.[27] Sample preparations were carried out in a glovebox (Plas-Labs) under an inert and dry atmosphere. Acetonitrile (AN), pyridine (Py), and dimethylformamide (DMF) (Aldrich) were dried over activated 3 Å molecular sieves (Sigma) according to Burfield et al.,[28,29] degassed, and transferred under vacuum. Tetrabutylammonium tetrafluoroborate (TBAF) was dried overnight in a vacuum oven at 80 °C. 1MeIm and DMAP, were of analytical grade from Aldrich and used as received either as a neat liquid or as a 1 M solution in AN/DMF, respectively.

Spectroscopic Titrations. Absorption spectra were recorded on a CARY 5 UV−visible−NIR spectrophotometer. Typically, 2 mL of 5 μM [Ni]-BChl solution in dry AN was placed in a 10-mm quartz cuvette that was sealed with a Teflon-coated rubber stopper. Ligands were injected through the septum with a microliter syringe. A set of 10−15 spectra at different ligand concentrations was recorded during each titration. Ligand binding constants, the pure spectra of [Ni]-BChl at each coordination state, and their confidence intervals were derived from the spectra as previously described.[2]

Electrochemical Measurements. Typically, electrochemical measurements required working with 100-fold more concentrated pigment solutions than spectroscopic measurement. To prevent aggregation and increase the solubility of [Ni]-BChl, we used AN containing 10% (v:v) DMF and 0.1 M TBAF (AN/DMF) as the electrolyte solution. The spectra of [Ni]-BChl in neat AN and the AN/DMF solution were identical (data not shown). Notably, the Q_x and B_y transition bands of [Ni]-BChl that are highly sensitive to axial ligation are identical in both solvents. Moreover, their peak positions (533 and 336 nm for Q_x and B_y, respectively) showed no indication of axial ligation by either DMF or AN to [Ni]-BChl.[2,25,27] Therefore we assumed that the ligation properties of [Ni]-BChl in the AN/DMF solution are the same as in neat AN.

Voltammograms were recorded on a BAS CV50w voltammetric analyzer. Square wave frequency, amplitude, and step-height were 50 Hz, 50 mV, and 2 mV, respectively. The electrochemical cell was a BAS low-volume cell with a standard three-electrode setup that was placed in the glovebox. The reference electrode was $Ag|Ag^+$ in an AN/DMF electrolyte solution. The working and counter electrodes were Pt disk and wire, respectively. A baseline of 1-mL clean electrolyte solution was measured and subtracted from the recorded voltammograms. Then, ferrocene (FeCp) was added and measured for use as an internal reference.[30] Afterward, [Ni]-BChl was added to the solution to make a concentration of about 0.5 mM, and another voltammogram was recorded. Finally, [Ni]-BChl was titrated with up to 90 μL of ligand in 8−10 steps. A voltammogram was recorded immediately after each titration step, and a sample of 50 μL was removed from the electrochemical cell. The sample's spectrum was recorded in a 0.1 mm-path length cuvette to monitor the coordination state of [Ni]-BChl[2].

Computational Methods. The conformational analyses of the molecular systems described here, including the structural and orbital arrangements as well as property calculations, were carried out using a variety of computational techniques for comparative purposes, using GAMESS[31] and GAUSSIAN98.[32] The primary methodology reported here are the hybrid density functional (HDFT) techniques.[33] More specifically, the HDFT functional used was B3LYP,[34] which employs the Lee−Yang−Parr correlation functional[35] in conjunction with a hybrid exchange functional first proposed by Becke.[36] HDFT techniques are particularly important for studies involving structures of the size considered here and have been previously shown by us[2] and others to be reliable for analysis of the type carried out here. The Hay and Wadt relativistic effective core potentials (RECP)[37] were used for the transition metal. The specific effective core potential/basis set combination chosen was LANL2DZ (Los Alamos National Laboratory 2-double-ζ; the "2" indicating that the valence and "valence-1" shells are treated explicitly).[38] The LANL2DZ basis set is of double-ζ quality in the valence and "valence-1" shells, whereas the RECP contains Darwin and mass-velocity contributions.[37,39,40] This RECP has been determined to be a computationally very efficient and reliable approach for handling relativistic effects, which must be accounted for in the complexes involving nickel.[41] In addition, the nature of each stationary point was uniquely characterized by analytically calculating and diagonalizing the matrix of energy second derivatives (Hessian) to determine the number of imaginary frequencies (0 = minima; 1 = transition state), which also provided the zero-point energies incorporated in the energy differences. For more accurate properties, fine-integration grid, tight single-point property calculations were carried out using a larger basis set denoted LANL2DZ+1, which consists of the LANL2DZ basis set augmented with single *f* functions (exponents determined by Frenkling and co-workers[42,43]) on Ni, and the standard Dunning's cc-pvdz (correlation consistent polarized valence double-ζ) basis set[38] ([4s3p1d/3s2p1d/2s1p]) on first- and second-row atoms. Extensive 3D molecular orbital analyses on all species were carried out using GAMESS/3D-PLTORB and were subsequently displayed using QMView.

Atomic charges are derived from a least-squares fit to the electrostatic potential (ESP) calculated at points selected according to the Merz−Singh−Kollman scheme,[44,45] and subject to the constraint of constant total molecular charge. A large number of points are thus chosen on nested Connolly surfaces with a density of 1 point/Å. The method samples points at 1.4, 1.6, 1.8, and 2.0 times the vdW radius of the atoms. Atomic radii were used (1.63 Å for Ni). Charge density difference plots were computed and analyzed using newly incorporated algorithms in GAMESS and QMView.[46]

The computations necessary for comparing with actual experimental results in solvent were performed using the polarizable conductor

(27) Hartwich, G.; Fiedor, L.; Simonin, I.; Cmiel, E.; Schafer, W.; Noy, D.; Scherz, A.; Scheer, H. *J. Am. Chem. Soc.* **1998**, *120*, 3675−3683.
(28) Burfield, D. R.; Lee, K. H.; Smithers, R. H. *J. Org. Chem.* **1977**, *42*, 3060−3065.
(29) Burfield, D. R.; Smithers, R. H.; Tan, A. S. C. *J. Org. Chem.* **1981**, *46*, 629−631.
(30) Gritzner, G.; Kuta, J. *Pure Appl. Chem.* **1983**, *56*, 461−466.
(31) Schmidt, M. W.; Baldridge, K. K.; Boatz, J. A.; Elbert, S. T.; Gordon, M. S.; Jensen, J. H.; Koseki, S.; Matsunaga, N.; Nguyen, K. A.; Su, S.; Windus, T. L.; Elbert, S. T. *J. Comput. Chem.* **1993**, *14*, 1347−1363.
(32) Frisch, M. J.; Trucks, G. W.; Schlegel, H. B.; Scuseria, G. E.; Robb, M. A.; Cheeseman, J. R.; Zakrzewski, V. G.; Montgomery, J. A., Jr.; Stratmann, R. E.; Burant, J. C.; Dapprich, S.; Millam, J. M.; Daniels, A. D.; Kudin, K. N.; Strain, M. C.; Farkas, O.; Tomasi, J.; Barone, V.; Cossi, M.; Cammi, R.; Mennucci, B.; Pomelli, C.; Adamo, C.; Clifford, S.; Ochterski, J.; Petersson, G. A.; Ayala, P. Y.; Cui, Q.; Morokuma, K.; Malick, D. K.; Rabuck, A. D.; Raghavachari, K.; Foresman, J. B.; Cioslowski, J.; Ortiz, J. V.; Stefanov, B. B.; Liu, G.; Liashenko, A.; Piskorz, P.; Komaromi, I.; Gomperts, R.; Martin, R. L.; Fox, D. J.; Keith, T.; Al-Laham, M. A.; Peng, C. Y.; Nanayakkara, A.; Gonzalez, C.; Challacombe, M.; Gill, P. M. W.; Johnson, B.; Chen, W.; Wong, M. W.; Andres, J. L.; Gonzalez, C.; Head-Gordon, M.; Replogle, E. S.; Pople, J. A. *GAUSSIAN 98*, Revision A.6; Gaussian, Inc.: Pittsburgh, PA, 1998.
(33) Parr, R. G.; Yang, W. *Density Functional Theory of Atoms and Molecules*; Oxford University Press: New York, 1989.
(34) Barone, V. *Chem. Phys. Lett.* **1994**, *226*, 392−398.
(35) Lee, C.; Yang, W.; Parr, R. G. *Phys. Rev.* **1988**, *B37*, 785−789.
(36) Becke, A. D. *J. Chem. Phys.* **1993**, *98*, 5648−5652.
(37) Hay, P. J.; Wadt, W. R. *J. Chem. Phys.* **1985**, *82*, 299−310.
(38) Dunning, T. H., Jr.; Hay, P. J. *Modern Theoretical Chemistry*; Plenum: New York, 1976.
(39) Hay, P. J.; Wadt, W. R. *J. Chem. Phys.* **1985**, *82*, 270−283.
(40) Wadt, W. R.; Hay, P. J. *J. Chem. Phys.* **1985**, *82*, 284−298.
(41) Siegbahn, P. E. M. *Adv. Chem. Phys.* **1996**, *93*, 333−387.
(42) Ehlers, A. W.; Boehme, M.; Dapprich, S.; Gobbi, A.; Hoellwarth, A.; Jonas, V.; Koehler, K. F.; Stegmann, R.; Veldkamp, A.; Frenking, G. *Chem. Phys. Lett.* **1993**, *208*, 111−114.
(43) Hoellwarth, A.; Boehme, M.; Dapprich, S.; Ehlers, A. W.; Gobbi, A.; Joans, V.; Koehler, K. F.; Stegmann, R.; Veldkamp, A.; Frenking, G. *Chem. Phys. Lett.* **1993**, *208*, 237−240.
(44) Besler, B. H.; Merz, K. M.; Kollman, P. A. *J. Comput. Chem.* **1990**, *11*, 431−439.
(45) Singh, U. C.; Kollman, P. A. *J. Comput. Chem.* **1984**, *5*, 129−145.
(46) Baldridge, K. K.; Greenberg, J. P. *J. Mol. Graphics* **1995**, *13*, 63−66.

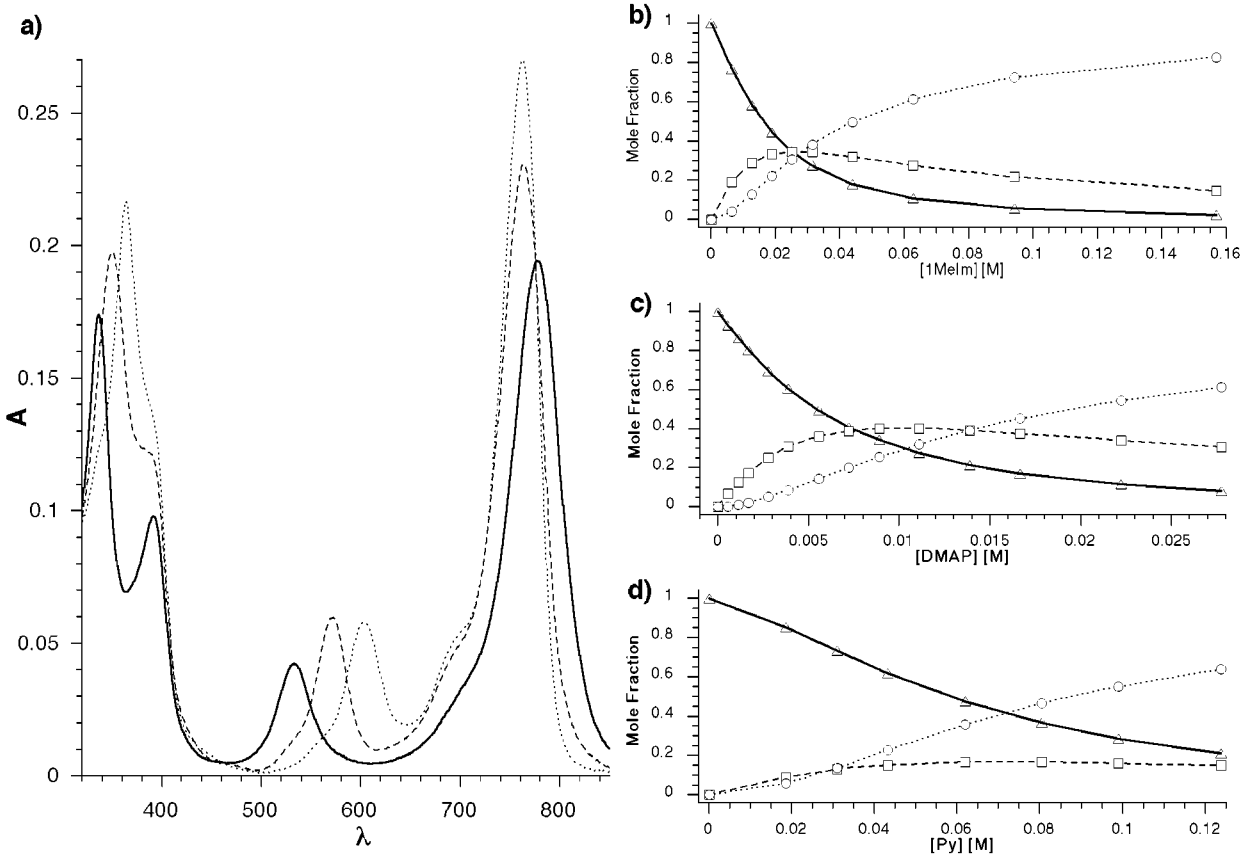

Figure 1. Spectra of [Ni]-BChl (—), [Ni]-BChl·1MeIm (- - -), and [Ni]-BChl·1MeIm$_2$ (···) in neat AN (a). Mole fractions of none- (—△—), mono- (- -□- -), and bi- (..○..), ligated [Ni]-BChl in AN as a function of 1MeIm (b), DMAP (c), and Py (d) concentrations.

Table 1. Absorption Peak Positions of Non-, Mono-, and Biligated Species of [Ni]-BChl in AN Derived from Spectroscopic Titrations of [Ni]-BChl with 1MeIm, DMAP, and Py Followed by Factor Analysis

	B_y [nm]	B_x [nm]	Q_x [nm]	Q_y [nm]
[Ni]-BChl	336	391	533	777
[Ni]-BChl·1MeIm	351	389	572	764
[Ni]-BChl·DMAP	350	387	571	764
[Ni]-BChl·Py	350	390	569	763
[Ni]-BChl·1MeIm$_2$	364	390	603	763
[Ni]-BChl·DMAP$_2$	364	390	601	762
[Ni]-BChl·Py$_2$	363	390	594	761

computational model,[47,48] at a dielectric permittivity of $\epsilon = 36.64$, as the value for acetonitrile. These computations were also performed using fine grid integration.

Results

Absorption spectra. Figure 1a presents the pure spectra of non-, mono-, and biligated [Ni]-BChl with 1MeIm as the ligand. The same absorption pattern is observed when the ligands are Py or DMAP. Table 1 presents the absorption maxima wavelengths[2] of the four main transition bands (Q_y, Q_x, B_x, and B_y, in order of increasing energy).

The mole fractions of non-, mono-, and biligated [Ni]-BChl as a function of 1MeIm, DMAP, and Py concentration are given in Figure 1, b, c, and d, respectively, and the corresponding ligand binding constants are given later in Table 3. Note that although ligand-binding constants increase with ligand nucleophilicity (DMAP > 1MeIm > Py), they do not necessarily correspond to the red shifts of the Q_x transition band (1MeIm > DMAP > Py) that is indicative of the amount of charge transferred from the ligand to the metal.[2] This distinction is made possible because the [Ni]-BChl system provides both the thermodynamic data (through concentration profile) and molecular data (through the spectroscopic transition energies).

Square-Wave Voltammetry. All redox potentials reported here are given in reference to the FeCp|FeCp$^+$ redox couple.[30]

Figure 2a presents voltammograms of [Ni]-BChl in AN/DMF with 0, 0.16, and 1.8 M 1MeIm. Similar voltammograms were recorded upon the addition of either Py or DMAP in place of 1MeIm. All voltammograms are typical of a reversible, two-step reduction of the BChl macrocycle.[49,50] Only a single peak for each reduction step was observed, even when the absoption spectra of non-, mono-, and biligated [Ni]-BChl was resolved, indicating the presence of a mixture. The peak positions of the first and second reduction potential (E_{1red} and E_{2red}, respectively) as a function of 1MeIm, DMAP, and Py concentration are given in Figure 2, parts b, c, and d, respectively.

The most notable ligand effect is a systematic negative shift of E_{1red} with increasing ligand concentration. The second reduction potential, E_{2red} is independent of the ligand concentration. The decrease in peak intensity can be attributed to

(47) Klamt, A. *J. Phys. Chem.* **1995**, *99*, 2224−2235.
(48) Baldridge, K.; Klamt, A. *J. Chem. Phys.* **1997**, *106*, 6622−6633.
(49) Watanabe, T. In *Electrochemistry of Chlorophylls*; Scheer, H., Ed.; CRC Press: Boca Raton, FL, 1991; pp 287−315.
(50) Geskes, C.; Hartwich, G.; Scheer, H.; Mantele, W.; Heinze, J. *J. Am. Chem. Soc.* **1995**, *117*, 7776−7783.

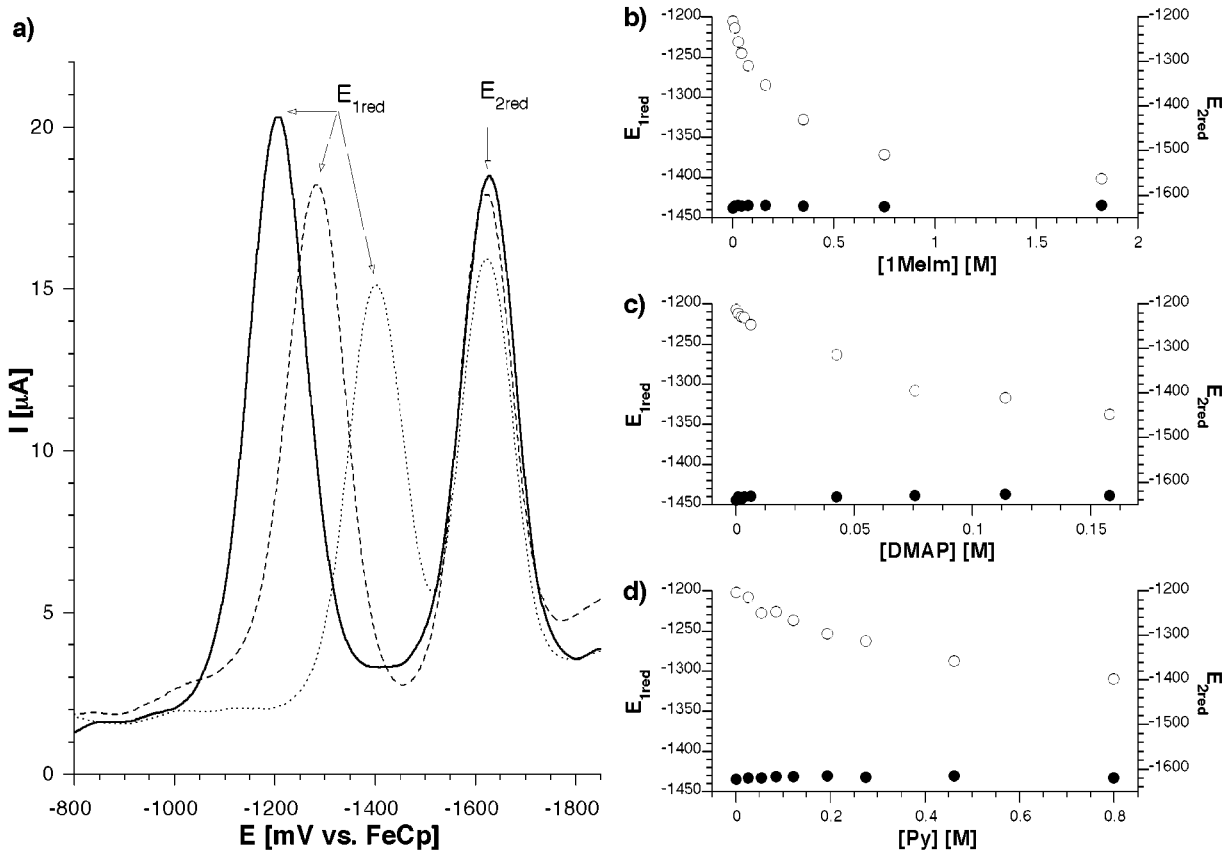

Figure 2. Voltammograms of [Ni]-BChl with 0 (—), 0.16 (- s- -), and 1.8 (···) M 1MeIm (a) in AN/DMF solution. E_{1red} (○) and E_{2red} (●) as a function of 1MeIm (b), DMAP (c), and Py (d) concentrations.

deterioration of the electrode response presumably due to ligand adsorption to the electrode surface. When the voltammograms were normalized to the same intensity for E_{1red} (not shown), we observed only slight offsets in the peak intensity of E_{2red} because of baseline instability at the far negative potentials.

Computational Results. The structures considered here were fully optimized and characterized with HDFT methods. The [Ni]-BChl macrocycle shows a ruffled conformation (Figure 3a), as expected for nickel(II) tetrapyrroles with an average Ni−N distances of 1.97 Å. This is an improvement in our theoretical structural prediction for Ni−N bond distance from previous work.[2] We found that our previously reported structure had small negative mode fluctuations (<65 cm^{-1}). Taking this into consideration leads to a more precise determination of the electronic structure with Ni−N bond length in much closer agreement to the experimental value. This results is similar to the value measured with EXAFS,[51] 1.95 ± 0.02 Å. Upon single axial ligation (i.e., imidazole) the molecule becomes almost planar (Figure 3b) with Ni−N average distance of 2.16 Å. Here, the four Ni−N distances break into classes, with the two longer bonds along the *Y* molecular axis and the two shorter bonds along the *X*-axis. In addition to the structural effects, ΔSCF calculation shows that the adiabatic electron affinity for [Ni]-BCl·Im is lowered by 0.33 eV compared to nonaxially ligated [Ni]-BChl. The axial ligand's lone pair in [Ni]-BChl·Im has a substantial occupation at the HOMO-2, as shown in Figure 3b.

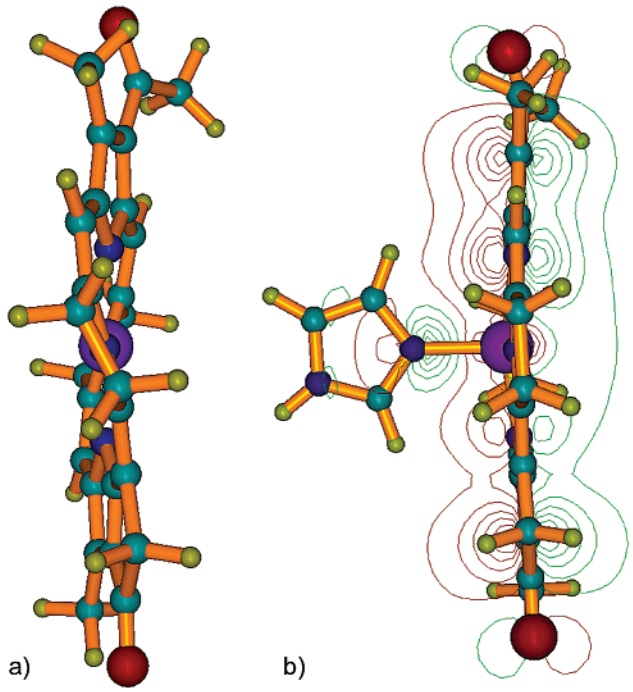

Figure 3. Side views of non- (a) and monoligated (b) [Ni]-BChl model compounds. Note the profound flattening of the macrocycle upon single imidazole molecule binding. Contours of MO HOMO-2 for the [Ni]-BChl·imidazole complex are plotted in the axial ligand plane.

The structure of the nonligated anion, [Ni]-BChl$^-$, is strongly ruffled with an average Ni−N distance of 1.97 Å, similar to the neutral complex.

(51) Chen, L. X.; Wang, Z.; Hatwich, G.; Katheder, I.; Scheer, H.; Scherz, A.; Montano, P. A.; Norris, J. R. *Chem. Phys. Lett.* **1995**, 437−444.

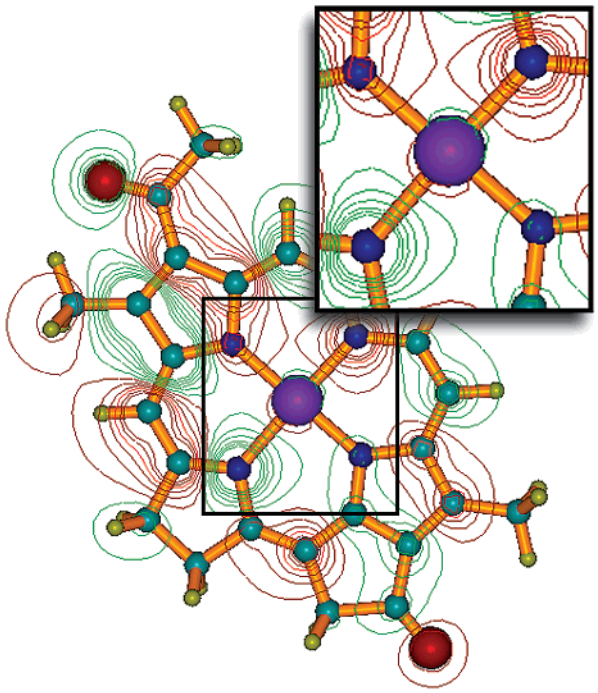

Figure 4. MO plot of [Ni]-BChl SOMO. Note the high occupation at two equatorial nitrogens and the small occupation at the nickel atom (inset).

Table 2. Changes in Covalent Radius, Ligation Energy, and Charge of Monoligated, Singly Reduced Monoligated, and Singly Reduced [Ni]-BChl with Respect to [Ni]-BChl

	[Ni]-BChl·Im	([Ni]-BChl·Im)$^-$	([Ni]-BChl)$^-$
Δr_{core}[Å][a]	+0.12	+0.11	−0.00(2)
ΔE_{lig}^{gas}[kcal/mol]	−15.8	−8.2	-
ΔE_{lig}^{solv}[kcal/mol]	−7.7	+2.0	-
ΔQ_{core}[e$^-$]	−0.29	−0.34	−0.18
ΔQ_{Im}[e$^-$]	+0.21	+0.15	-

[a] Change in the mean equatorial Ni−N distance between the corresponding species and [Ni]-BCHhl.

The [Ni]-BChl anion's SOMO (Figure 4), exhibits mainly a π character, similar to the Gouterman's LUMO orbital (it also shows a small, yet nonnegligible amplitude at the metal site (inset, Figure 4)). Therefore, the reduced complex should be regarded as [Ni]-BChl π anion radical, in-line with previous spectroelectrochemical measurements of reduced [Ni]-BChl in THF.[50] This is also reflected in the fact that the anion core does not show an increase in the average Ni−N distance. Furthermore, the calculated distances for the axially ligated π anion radical [Ni(II)]-BChl$^-$·imidazole, are close to those derived for the high-spin [Ni(II)]-BChl·imidazole (Table 2).

For a zero-order approximation, both photoexcitation and electroreduction involve occupying the lowest unoccupied molecular orbital (LUMO), which consequently increases the electron density at the equatorial nitrogens.

Computationally, we find that the ligation energy for an axial Imidazole in the neutral and reduced complexes is −15.8 and −8.2 kcal/mol, respectively, in the gas phase. Upon reduction the ligand−metal distance is increased by 0.32 Å. When solvation is considered, the energy of ligation for the singly reduced species becomes positive (+2.0 kcal/mol); thus, dissociation is predicted.

Scheme 2

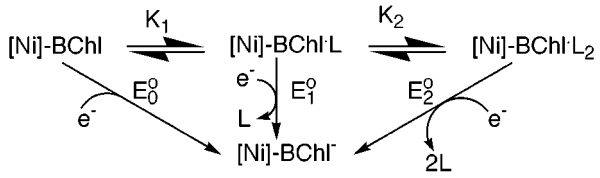

Discussion

Axial Ligand Dissociation from Reduced [Ni]-BChl. The strong dependence of E_{1red} on ligand concentration and the invariance of E_{2red} suggest that the first reduction of mono- and biligated [Ni]-BChl leads to ligand dissociation, as described in Scheme 2. Additionally, the reversible voltammetric signals indicate that ligand association and dissociation processes are much faster than the heterogeneous electrode reactions (that are nevertheless, Nernstian).

Therefore, we derive a model based on the standard semiempirical formalism of steady-state mass transfer[52] for the dependence of E_{1red} on the ligand concentration. The reduction current, i, is given by

$$i = m{\cdot}F{\cdot}A{\cdot}[(C_4^* - C_4^\circ) + (C_5^* - C_5^\circ) + (C_6^* - C_6^\circ)] \quad (1)$$

where m, F, and A are the mass transfer coefficient, Faraday constant, and electrode area, respectively, C_4^*, C_5^*, and C_6^* are the initial bulk concentrations of non-, mono, and biligated [Ni]-BChl, respectively, and C_4°, C_5°, and C_6° are the respective concentrations at the electrode surface. Substituting, according to Scheme 2, $C_5 = K_1{\cdot}[L]{\cdot}C_4$, and $C_6 = K_1{\cdot}K_2{\cdot}[L]^2{\cdot}C_4$, where [L] is the ligand concentration yields

$$i = m{\cdot}F{\cdot}A{\cdot}\mathscr{R}{\cdot}(C_4^* - C_4^\circ) \quad (2)$$

where $\mathscr{R} \equiv 1 + K_1{\cdot}[L] + K_1{\cdot}K_2{\cdot}[L]^2$.

Because of the fast ligand dissociation, the only reduced species produced at the electrode is [Ni]-BChl$^-$ and therefore

$$i = m{\cdot}F{\cdot}A{\cdot}(C_{4-}^\circ - C_{4-}^*) = m{\cdot}F{\cdot}A{\cdot}C_{4-}^\circ \quad (3)$$

where C_{4-}° is the [Ni]-BChl$^-$ concentration at the electrode and C_{4-}^* is its bulk concentration that is initially zero. Substituting eqs 2 and 3 into the Nernst equation for one-electron half-reaction (at 25 °C),

$$E = E_0^\circ + 59.1{\cdot}\log{\cdot}(C_4^\circ/C_{4-}^\circ) \quad (4)$$

where E is the electrode potential and E_0° is the standard potential for the [Ni]-BChl/[Ni]-BChl$^-$ couple, in mV, yields

$$E = E_0^\circ - 59.1{\cdot}\log(\mathscr{R}) + 59.1{\cdot}\log[(i_l - i)/i] \quad (5)$$

where i_l is the limiting current given by $i_l = m{\cdot}F{\cdot}A{\cdot}\mathscr{R}{\cdot}C_4^*$. The half-wave potential is

$$E_{1red} \equiv E(i = i_l/2) = E_0^\circ - 59.1{\cdot}\log(\mathscr{R}) = E_0^\circ - 59.1{\cdot}\log(1 + K_1{\cdot}[L] + K_1{\cdot}K_2{\cdot}[L]^2) \quad (6)$$

Figure 5 illustrates curve fits of eq 6 with L ≡ 1MeIm, DMAP, and Py for K_1 and K_2 values derived from the

(52) Bard, A. J.; Faulkner, L. K. *Electrochemical Methods. Fundamentals and Applications*; John Wiley: 1980.

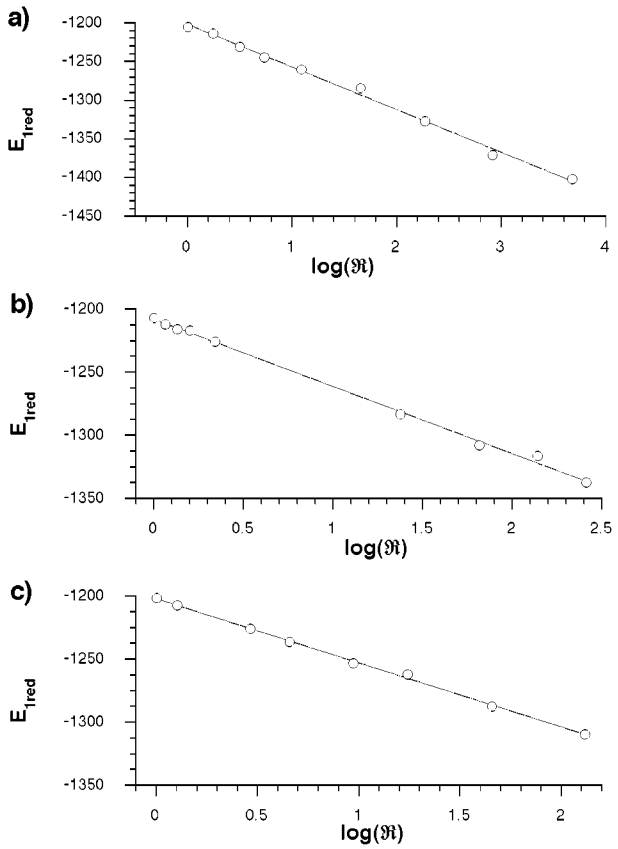

Figure 5. E_{1red} vs log($\mathscr{R}$) plots for [Ni]-BChl with 1MeIm (a), DMAP (b), and Py (c).

spectroscopic titrations. As shown in Table 3, the correlation coefficients (R^2) for all three cases are larger than 0.995, the slopes are close to the theoretical value (59.1 mV), and the intercepts yield $E_0^\circ = -1204 \pm 5$ mV.

Alternatively, the maximum-likelihood values of K_1 and K_2 can be obtained by minimizing the RMS error function given by

$$\mathrm{RMSE}(K_1,K_2) = \sqrt{\sum_i [E_i - (a\cdot\log(\mathscr{R}_i) + b)]^2/m}, \quad (7)$$

where E_i and $\mathscr{R}_i$ are the experimental E_{1red} and $\mathscr{R}$ at a ligand concentration $[L]_i$, respectively, m is the number of experimental data points, and a and b are the respective slope and intercept of the straight line obtained from a least-squares fit of $\{log(\mathscr{R}_i)\}$ to $\{E_i\}$.

Table 3 shows that although slopes, intercepts, and correlation coefficients obtained by using the maximum-likelihood approach are similar to those obtained by using the spectroscopically derived ligation constants, the maximum-likelihood method resulted in too large confidence intervals for K_1 and K_2. This is because of the logarithmic dependence of E_{1red} on K_1 and K_2.

Thus, unless eq 6 can be simplified to a linear form (e.g., assuming $K_1\cdot[L] \ll K_1\cdot K_2\cdot[L]^2 \gg 1$ yields $E_{1red} = E_0^\circ - 59.1\cdot\log(K_1\cdot K_2) - 118.2\cdot\log([L])$[53]), spectroscopic titrations remain the preferred method for providing accurate ligand binding constants.

(53) Nesset, M. J. M.; Shokhirev, N. V.; Enemark, P. D.; Jacobson, S. E.; Walker, F. A. *Inorg. Chem.* **1996**, *35*, 5188−5200.

Axial Ligand Dissociation Mechanism. A mechanism was proposed for the photoinduced axial ligand dissociation in Ni-porphyrins involving ultrafast photoexcitation energy transfer from the lowest $\pi-\pi^*$ excited state of the macrocycle to the central Ni atom, thereby changing its electronic configuration from a high-spin ($^1d_{x^2-z^2}$, $^1d_{z^2}$) triplet state to a low-spin ($^2d_{z^2}$) singlet state. In that mechanism, ligand dissociation follows, because of the strong repulsion between the doubly occupied d_{z^2} orbital and the electron density on the axial ligands. As mentioned, electroreduction in nickel porphyrins is metal-centered and also results in a ($^1d_{x^2-z^2}$, $^2d_{z^2}$) electronic configuration. Therefore, in this case the analogy to photodissociation is straightforward. However, as outlined above, this mechanism, which applies to Ni-porphyrins, cannot explain axial ligand dissociation from [Ni]-BChl, where the reduction results in a π anion radical. Apparently, axial ligand dissociation from [Ni]-BChl, which involves breaking a σ bond, appears to be driven by modulation of the equatorial ligand's π system.

To account for these experimental results, we propose a new mechanism. In our previous studies we showed that upon axial ligand binding, electron density migrates to the equatorial nitrogens and the Ni atom ([Ni]-BChl core area).[2] Here we show that electron migration to the central core also occurs upon electro-reduction. Similar charge migration to the central core occurs when the LUMO of [Ni]-BChl is populated by photo-excitation. Thus, the concomitant ligation and reduction (or photoexcitation) cause electrostatic repulsion at the core area of [Ni]-BChl. Ligand dissociation then allows for relaxation of that repulsion. This simple electrostatic picture can explain both photo- and electro-induced axial ligand dissociation in [Ni]-BChl. The electrostatic interaction is the origin of the $\sigma-\sigma$ communication, and it is not restricted by orbital overlap or symmetry considerations. The interplay of the π- and σ-electronic systems in controlling the metal−ligand affinity is intriguing and may be relevant to biological catalysis.

The mechanistic approach proposed here is based on charge repulsion and highlights the driving force for ligand dissociation. In all three species ([Ni]-BChl$^-$, [Ni]-BChl*, and [Ni]-BChl$\cdot$L) excess charge density is directed toward the core area; therefore, any two species are mutually exclusive (i.e. ([Ni]-BChl$\cdot$L)$^-$ is less stable than [Ni]-BChl$\cdot$L). The QM calculations performed for the [Ni]-BChl complexes confirm this. The total charge density difference plot (Figure 6) shows a marked modification of the electron density distribution in the [Ni]-BChl core upon reduction. The Merz−Singh−Kollman charge analysis for the reduced, and ligated [Ni]-BChl shows an increase of 0.18 and 0.29 electron charge units, for the total charge located on the core nitrogen atoms and metal, respectively (Table 2). The charge is accumulated to a large extent in the core area, although the [Ni]-BChl anion SOMO is predominantly of π character. Furthermore, the charge analysis (in the gas phase) shows that the imidazole ligand transfers 0.15 and 0.21 electron charge units to the rest of the complex in ([Ni]-BChl$\cdot$imidazole)$^-$ and [Ni]-BChl$\cdot$imidazole, respectively.

Hence, it appears that the core in the reduced complex is less suitable for further σ-charge donation. These data, combined with the reduced ligation energy (from −15.8 to −8.2 kcal/mol) and the increased ligand−metal distance (by a calculated 0.32 Å), predicts partial ligand dissociation for the nonsolvated complex. Computationally, we find that complete ligand dis-

Table 3. Binding Constants for the First (K_1) and Second (K_2) Ligands and Standard Reduction Potentials Non-, Mono-, and Biligated [Ni]-BChl (E_0°, E_1°, and E_2°, Respectively)

	1MeIm		DMAP		Py	
	spectroscopy[a]	maximum likelihood[b]	spectroscopy[a]	maximum likelihood[b]	spectroscopy[a]	maximum likelihood[b]
K_1	39.7 ± 0.9	34^{+42}_{-18}	131 ± 2	123^{+126}_{-63}	5.7 ± 0.2	8^{+3}_{-2}
K_2	35.5 ± 0.9	30^{+64}_{-23}	72.1 ± 0.9	135^{+278}_{-110}	34.6 ± 0.9	23^{+14}_{-10}
slope[c]	-55 ± 1	-57 ± 1	-53 ± 1	-48.2 ± 0.8	-50.7 ± 0.9	-51.4 ± 0.7
R^2[d]	0.9954	0.9958	0.9976	0.9979	0.9986	0.9987
E_0° [mV]	-1202 ± 3	-1204 ± 3	-1208 ± 1	-1208 ± 1	-1202 ± 1	-1201.4 ± 0.8
E_1° [mV][e]	-1297 ± 6		-1329 ± 5		-1249 ± 6	
E_2° [mV][e]	-1390 ± 6		-1439 ± 6		-1340 ± 7	

[a] Ligand binding constants derived from the spectroscopic titrations. [b] Ligand binding constants derived by minimizing eq 7. [c] E_{1red} vs $\log(1 + K_1 \cdot [L] + K_1 \cdot K_2 \cdot [L]^2)$ where [L] is the axial ligand concentration. [d] Correlation coefficient. [e] From eq 8 using $E_0^\circ = 1204 \pm 5$.

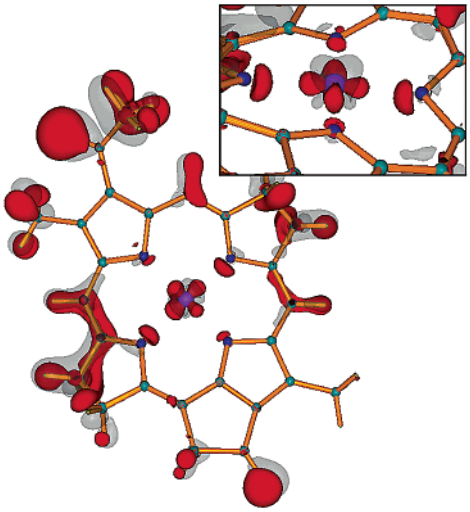

Figure 6. The total density difference calculated for [Ni]-BChl (anion−neutral). Red and gray isosurfaces indicate an excess and depletion of electron density, respectively in the anion species, compared with the neutral species (top). Inset shows the core area (side view).

sociation is predicted only when considering solvation. This result, which is in line with the electrochemical measurements, provides an insight as to the role played by the environment in the completion of the dissociation process.

To summarize, our studies show that coordination of equatorial and axial ligands is mutually modulated by changing the electron density around the metal. Migration of electron density to the metal center in the equatorial plane increases the axial ligand−metal distance and *vice versa*. Such a change in charge distribution may be induced by photoexcitation, electroreduction, or any modification of peripheral side groups that may alter the partial negative charge at the equatorial plane in vicinity to the core area. The common basis for the dissociative effect of reduction and photoexcitation[54−56] shown here, stresses the relevance of using ultrashort light pulses[57−60] for triggering metal-centered catalytic processes.

Redox Tuning and Control in [Ni]-BChl by Axial Ligation. As shown above, reduction of non-, mono-, and biligated [Ni]-BChl is adequately described by the thermodynamic cycle in Scheme 2, whereby reduction of the equatorial π system and axial ligand dissociation occur simultaneously. Consequently, the standard reduction potentials of mono- and biligated [Ni]-BChl, E_1°, and E_2°, respectively, are determined by E_0°, and the ligand binding constants K_1 and K_2 according to the Nernst equation

$$E_0^\circ = E_1^\circ + 59.1 \cdot \log(K_1) = E_2^\circ + 59.1 \cdot [\log(K_1) + \log(K_2)] \quad (8)$$

Table 3 shows that each additional ligand makes [Ni]-BChl harder to reduce by 50−150 mV.

The $\sigma-\pi$ coupling described in the proposed mechanism above, is manifested both thermodynamically and by a 0.33 eV lowering of the adiabatic electron affinity of [Ni]-BChl·Im compared to the nonaxially ligated complex.

In conclusion, axial ligand association/dissociation modifies both the redox potential of the Ni complex and the macrocycle geometry. The interplay between charge repulsion at the metal center and structural modification of the equatorial ligand may provide the means for tuning the catalytic cycle of metal redox reactions by the protein environment. The activation of F430 in MCR may be one example in which such a mechanism is employed.

Application to F430. Crystallographic and spectroscopic data show a dynamic coordination sphere around the Ni center for the different states of MCR. The oxygen of a glutamine residue occupies one axial position (the "proximal" position); the other axial position (the "distal" position) is occupied by the sulfonate oxygen, thiol group of the coenzyme M substrate, or possibly other ligands.[21,61]

Recently, Telser et al.[21] suggested that activation of the MCR F430 complex involves a reduction of Ni(II) into Ni(I) and dissociation, or partial dissociation of at least one axial ligand. This proposal is backed by a comparison with model compounds that have similar or even identical paramagnetic properties to those found for the cryogenically reduced MCR complex. However, it is not clear which ligand dissociates and what is the intermediate coordination sphere of the Ni cation. Thus, elucidating the role played by axial ligands in the catalytic cycle of F430 is important for understanding the catalytic function of the metal center.

(54) Rodriguez, J.; Holten, D. *J. Phys. Chem.* **1990**, *92*, 5944−5950.
(55) Eom, H. S.; Jeoung, S. C.; Kim, D.; Ha, J. H.; Kim, Y. R. *J. Phys. Chem. A* **1997**, *101*, 3661−3669.
(56) Uesugi, Y.; Mizutani, Y.; Kitagawa, T. *J. Phys. Chem. A* **1998**, *102*, 5809−5815.
(57) Srajer, V.; Teng, T. Y.; Ursby, T.; Pradervand, C.; Ren, Z.; Adachi, S.; Schildkamp, W.; Bourgeois, D.; Wulff, M.; Moffat, K. *Science* **1996**, *274*, 1726−1729.
(58) Dellalonga, S.; Ascone, I.; Fontaine, A.; Castellano, A. C.; Bianconi, A. *Eur. Biophys. J.* **1994**, *23*, 361−368.
(59) Nakashima, S.; Kitagawa, T.; Olson, J. S. *Chem. Phys.* **1998**, *228*, 323−336.
(60) Park, S.; Pan, L. P.; Chan, S. I.; Alben, J. O. *Biophys. J.* **1996**, *71*, 1036−1047.
(61) Ermler, U.; Grabarse, W.; Shima, S.; Goubeaud, M.; Thauer, R. K. *Science* **1997**, *278*, 1457−1462.

In accordance with our findings with [Ni]-BChl, we propose that axial ligand association/dissociation to the Ni center in MCR has two major functions: (1) it controls the dimension of the central core and the planarity of the macrocycle as described above, and (2) it modulates the electron density at the Ni center. Ultimately, these functions allow for efficient structural and electronic tuning of the Ni center for alternate steps of reduction and substrate binding during the catalytic cycle. To further resolve the suggested contribution of axial ligation, we have listed below relevant observations concerning F430 in vitro and in vivo.

EXAFS and X-ray studies of low-spin Ni(II)-F430M and its 12,13-diepimer showed short average Ni−N distances in both complexes (∼1.90A, with a slightly shorter distance for the diepimer complex).[62,63] Coordination of two axial ligands to the Ni(II) center in isolated F430 expands the Ni−N distance by ∼0.2 Å to approximately 2.1 Å.[62,64] A similar average Ni(II)−N distance was observed by X-ray crystallography at high resolution for F430 within the MCR protein.[24] The macrocycle of F430 in $MCR_{ox1-silent}$ and $MCR_{red1-silent}$ is relatively planar and similar in geometry to the axially biligated 12,13-diepi F430M in vitro.[63]

Thus, axial ligation appears to cause ∼0.2 Å expansion of the central core in F430, similar to the value found for other Ni(II) tetrapyrrole systems both in vitro and in vivo. Reduction of Ni(II) to Ni(I), for example, in Ni F430M (pentamethyl ester of F430) also shows an average core expansion of about 0.2 Å with two sets of Ni−N distances.[62] Ni(I) F430M, like other Ni(I) tetrapyrroles, shows low affinity to axial ligands. Nevertheless, in some cases it was found that Ni(I) tetrapyrroles can loosely bind axial ligands, for example in the pyridine−Ni(I)octaethylisobacteriochlorin complex where the Ni−N pyridine distance of 2.2 Å was determined by EXAFS.[65]

In our study we found that coordination of [Ni(II)]-BChl to one axial ligand was sufficient to bring the molecule to an essentially planar configuration, with an average Ni−N distance of 2.16 Å compared with 1.97 Å in the nonligated [Ni]-BChl complex.

The increase of 0.19 Å found by us for [Ni(II)]-BChl compares well with the ∼0.20 Å difference between the Ni−N average distance in ligated and nonligated forms of the F430 models. This holds for the bromide salt of 12,13-diepi F430M, and F430M. Notably, the Ni−N average distance (2.08 Å) found for $MCR_{ox1-silent}$[24] agrees well with the distance found for the isolated, hexa-coordinated F430. Thus, it appears that in all F430 complexes axial ligation is a dominant factor in controlling the macrocycle conformation. However, we do not rule out the contribution of peripheral substituents and stereochemistry to the molecule's geometry.[66] Computationally, we found that reduction of the π system in the [Ni(II)]-BChl·imidazole complex, although weakening the ligand binding and elongating the Ni−N distance by 0.32 Å, did not alter the expanded core configuration induced by the axial ligand (the nonligated reduced complex shows a ruffled conformation and short Ni−N distances similar to the neutral nonligated complex). This result, obtained for the reduced complex in the gas phase, may be highly relevant for a "gas-phase" environment[24] within the niche of the protein active site. Furthermore, it scores the microscopic role of protein solvation in controlling quasi-stable states during the catalytic cycle, including the final dissociation of the axial ligand. Considering these observations and related computations, we suggest that even a weakly bound axial ligand may have a substantial effect on the macrocycle conformation. Namely, binding of the F430 cofactor to an axial glutamine residue may have an important structural role in preparing the complex to the reduced state. The coordinating environment in the MCR catalytic niche is probably designed in a way that ensures smooth adiabatic transition between the different Ni redox states, where the structural modifications of the macrocycle are arranged before the reduction process. Moreover, the peripheral hydrogen-bonding network may have an additional structural influence on the macrocycle conformation.[24]

Reduction is expected to be accompanied by partial dissociation of one of the axial ligands (the glutamine residue or the thiol group) because of electron density accumulation at the metal core and the aforementioned electrostatic repulsion. Here, a small increase in the axial Ni−ligand distance (0.2−0.3 Å) may be sufficient. This partially dissociative configuration may apply to the MCR_{red1} form proposed by Telser et al. We presume that this form is a short-living species because of the protein environment constraints and possibly, the presence of an electron acceptor. Therefore, the partially dissociated F430 intermediate rapidly relaxes to the silent, biligated form. In addition to the structural details discussed here, special attention should be given to the redox tuning of the metal center via axial ligation. As we showed, both from the experimental thermodynamic data and from the QM calculations, axial ligation has a substantial effect in determining the redox potentials or electron affinity of the Ni center.

(62) Furenlid, L. R.; Renner, M. W.; Fajer, J. *J. Am. Chem. Soc.* **1990**, *112*, 8987−8989.
(63) Farber, G.; Keller, W.; Kratky, C.; Jaun, B.; Pfaltz, A.; Spinner, C.; Kobelt, A.; Eschenmoser, A. *Helv. Chim. Acta* **1991**, *74*, 697−716.
(64) Shiemke, A. K.; Kaplan, W. A.; Hamilton, C. L.; Shelnutt, J. A.; Scott, R. A. *J. Biol. Chem.* **1989**, *264*, 7276−7284.
(65) Renner, M. W.; Furenlid, L. R.; Stolzenberg, A. M. *J. Am. Chem. Soc.* **1995**, *117*, 2379−2379.

(66) In recent computational studies *(J. Phys. Chem. B* **2000**, *104*, 10858−10862*; J. Am. Chem. Soc.* **2000**, *122*, 6375−6381*)* Ghosh et al. claim that the native stereochemistry of Ni(II)F430 (with no axial ligands) induces flattening of the macrocycle and core expansion, which provides stabilization of the Ni(I) state. Their suggestion is based on the relatively flat macrocycle conformation that they calculated for Ni(I)- and Ni(II) (low spin) F430′ (a model compound where the acetate, acetamide, and propionate side-chains of F430 were simplified to methyl groups) compared to the ruffled geometry of its 12,13 diepimer. Specifically, they found that Ni(II)F430′ has ruffling angles of 13.78, 20.75, 36.24, and 27.31 and an average Ni−N distance of 1.99 A. For the 12,13 diepimer (Ni(II)-diepi-F′430), they found a much more ruffled conformation with ruffling angles of 34.28, 45.17, 59.91, and 50.04 and an average Ni−N distance of 1.93Å. As mentioned above, the profound differences between the two conformations were attributed to the native stereochemistry of the F430 macrocycle. Generally, it appears that the computational work was performed well in this study, and as stated "*...tight convergence criteria for atomic forces and displacements in the geometry optimizations... for the highest component of the nuclear gradient...*". Nevertheless, we would like to note that with a highly flexible macrocycle such as F430, extra caution should be exercised when trying to elucidate fine structural details by QM computations. From our own experience with [Ni]-BChl, we found that small negative mode fluctuations may lead to the wrong macrocycle conformation determination. Thus, unless the nature of the stationary point found is characterized by calculating and diagonalizing the matrix of energy second derivatives, a relatively flat macrocycle conformation with an average Ni−N distance of 2.00 Å is calculated for [Ni(II)]-BChl. The energy of this conformation is close to the real minimum of [Ni(II)]BChl ($\Delta E = \sim 2.3$ kcal/mol) for which the average Ni−N distance is 1.97 Å and the dihedral ruffling angles are −27.52°, −26.45°, 32.80°, and 29.19° (this work). We suspect that the average Ni−N distance provided by Ghosh et al. for low-spin Ni(II)-F′430 (1.99 Å) may reflect a saddle point rather than a true energy minimum configuration. This may account for the discrepancy between the experimentally determined Ni−N average distance for low-spin Ni(II)-F430M *(*1.90 Å, *J. Am. Chem. Soc.* **1990**, *112* 8987−8989*)* and the value calculated by Ghosh et al.

The emerging dynamic role of axial ligands in the catalytic cycle of F430, as exemplified here, agrees well with recent mechanisms proposed on the grounds of experimental studies.[21,24]

Conclusions

We have proposed a mechanism whereby the equatorial ligand (the BChl π system) regulates the metal's reactivity and affinity to axial ligands by changing the partial charges at the [Ni]-BChl core. The proposed mechanism accounts for the initiation of ligand dissociation in [Ni]-BChl observed upon both photoexcitation and electroreduction. Repulsive interactions at the [Ni]-BChl core area between the excess electron density donated by axial and equatorial ligands makes ligand binding and photoexcitation, or electroreduction mutually exclusive. However, solvation of the products is required in order to accomplish the dissociation process.

The proposed mechanism may be highly relevant to the catalytic function of metal centers in enzymes where ligand binding may be used as a thermodynamic trigger for biological redox reactions.

It is commonly assumed that controlling the catalytic activity of metal tetrapyrrole complexes within the protein milieu requires two axial ligands: one for the actual binding of the substrate and the other for regulating the catalytic activity, for example, by using the trans-effect.[13] On the basis of our findings, we suggest that modification of the charge distribution at the regulating ligand brings the axial ligand to a predissociative state.

We have shown quantitatively that axial ligands modify the electron density at the metal center and control the macrocycle geometry in [Ni]-BChl using the recently described molecular potentiometer.[2] We propose that axial ligands affect the catalytic action of biological metal centers by controlling the equatorial ligand geometry and charge distribution, and *vice versa*. This principle was demonstrated in the MCR complex where the geometry of F430 has to adopt alternate redox states of the central metal. In continuing our study, current efforts in our laboratory are aimed at rigorous computational analyses of F430 model compounds at different coordination and redox states.

Further experimental and computational studies aimed at perusing the generality of the proposed mechanism are in progress.

Acknowledgment. This research was supported by a U.S.−Israel Binational Science Foundation Grant (9800323), a Sonder-Forschungsbereich Grant (533), the Willstatter-Avron-Minerva Foundation for Photosynthesis, and the NIH NBCR (RR08605-06). A.S. is an incumbent of the Yedle and Robert Sclare Chair for Biochemistry. We would like to thank J. P. Greenberg for his visualization expertise.

JA0121078